Fracture behavior and mechanical characterization of R350HT rail steel

Leonetti, Davide; Ferreira, Vitória Mattos; Schotsman, Bart

DOI
10.1016/j.prostr.2023.07.015

Publication date
2023

Document Version
Final published version

Published in
Procedia Structural Integrity

Citation (APA)
Leonetti, D., Ferreira, V. M., & Schotsman, B. (2023). Fracture behavior and mechanical characterization of R350HT rail steel. *Procedia Structural Integrity*, *47*, 219-226. https://doi.org/10.1016/j.prostr.2023.07.015

Available online at www.sciencedirect.com

ScienceDirect

Procedia Structural Integrity 47 (2023) 219–226

Structural Integrity Procedia

www.elsevier.com/locate/procedia

27th International Conference on Fracture and Structural Integrity (IGF27)

Fracture behavior and mechanical characterization of R350HT rail steel

Davide Leonetti[a,*], Vitória Mattos Ferreira[b], Bart Schotsman[b,c]

[a] *Eindhoven University of Technology, Eindhoven, The Netherlands*
[b] *Delft University of Technology, Delft, The Netherlands*
[c] *ProRail, Utrecht, The Netherlands*

Abstract

R350HT is a standard premium heat-treated rail steel and the reference for new rail steel development. The present study discusses an experimental characterization of fatigue crack growth rate and fracture toughness for this refined pearlitic rail steel in mode-I-loading. The tests are carried out on compact tension specimens extracted from the rail head with the straight notch pointing to the rail foot. As a result, the crack path orientation approximates deep rolling contact fatigue cracks. The fracture surfaces obtained under cyclic and monotonic loading are compared by means of scanning electron microscopy. The results are analyzed and discussed with reference to the morphology of the fracture surfaces for the crack initiation sites, fatigue crack growth region, and the final fracture region, evidencing the role of the microstructure, and inclusions on the fracture behavior. From the analysis of the crack path and fracture surface, it is concluded that the refined microstructure and ferrite ductility play an important role in fracture behavior.

Keywords: R350HT; fatigue crack growth rate; fracture toughness

1. Introduction

The increasing traffic load and intensity on the railway network require the use of high-strength and wear-resistant rail steels, in order to guarantee the safe use of the rail infrastructure. Railway rails are subjected to localized and high contact forces, inducing slipping mechanisms, and adverse weather conditions, causing wear, rolling contact fatigue, and other rail-related damage phenomena Lichtberger (2011); Zerbst et al. (2009). The shift to steel grades characterized by higher wear resistance makes the growth of rolling contact fatigue cracks more prone to induce failures. In other words, a competition exists between these two phenomena, i.e. rolling contact fatigue and wear, such that they compete with each other, despite the accumulation of plastic strain being the reason for both phenomena Cannon and

* Corresponding author.
E-mail address: d.leonetti@tue.nl

10.1016/j.prostr.2023.07.015

Pradier (1996); Christoforou et al. (2019); Kapoor (1997). Advances in chemical composition and production routes of railway steels allow for obtaining rail steel grades with improved strength and wear resistance. One example is the R350HT steel grade which is widely used in switches, crossings, and curved tracks because of its increased service life. The improved properties with respect to standard-grade steel are mainly the result of fast cooling after hot rolling leading to a small interlamellar spacing of the pearlitic structure, resulting in high hardness and strength.

The relevance of characterizing the fracture resistance and the material behavior of railway rails is also due to the large variety of cracks that can potentially nucleate, and the complex state of stress to which these cracks are subjected Zerbst et al. (2005); Pucillo et al. (2021). With respect to this, several methods and models have been developed to be able to estimate the severity of the stress state at the tip of fatigue cracks, formulating finite element models, or weight function solutions Olzak et al. (1991); Bogdanski et al. (1996); Bogdański et al. (1999); Farjoo et al. (2012); Trollé et al. (2012); Pucillo et al. (2019); Leonetti and Vantadori (2022b,a).

It is well known that pearlitic steels are characterized by a brittle behavior under quasi-static loading conditions at room temperature Rosenfield et al. (1972). This generally results in relatively low damage tolerance properties, i.e. relatively high fatigue crack growth rate and low fracture toughness at the service temperature, Pucillo (2022). On the contrary, monotonic tensile stress-strain curves and S-N curves are such that static and fatigue strength properties can be qualified as relatively high Masoudi Nejad et al. (2020), since rail steels have Brinell Hardness values, between 260 and 400 HB.

Therefore, characterizing the fracture resistance in terms of fatigue crack growth and fracture toughness of rails steels allows for assessing the damage tolerance of railway rails. Moreover, the study of the fracture behavior through the investigation of the fracture surfaces supports the further development of rail steels. This paper shows a dedicated experimental investigation on R350HT steel. In particular, monotonic tensile tests have been conducted on coupons extracted from the rail head. The same coupons are examined both at the fracture surface and longitudinal section to corroborate the information from the tensile test, in terms of fracture behavior. In addition, plane strain fracture toughness tests and fatigue crack growth rate tests have been conducted to quantify fracture mechanics properties and compare them with similar steel grades.

Nomenclature

a	Crack depth
B	Thickness of the compact tension C(T) specimen
E	Young's modulus
K_{IC}	Plane strain mode-I fracture toughness
K_I	Mode-I stress intensity factor
K_{Isi}	Size insensitive plane strain mode-I fracture toughness
K_Q	Fracture toughness
P	Applied load
R	Load ratio
S_Q	Secant offset percentage to calculate P_Q in the $P-v$ curve
u	Elastic compliance
v	Crack mouth opening displacement
W	Width of the C(T) specimen

2. Experimental investigation

2.1. Material

In this study, all tests were carried out on R350HT railway steel fresh from the rolling mill (not used on track). This steel grade has a close-to-eutectoid chemical composition with 0.77 wt.% of C, 1.10 wt.% of Mn and 0.39 wt.% of Si and an average hardness of 355 ± 8 HV.

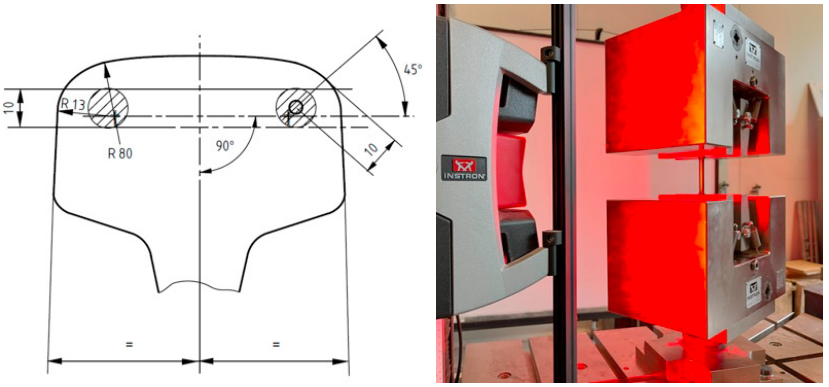

Fig. 1: Location and dimensions (mm) of tensile specimens (left) and experimental test setup (right)

2.2. Monotonic tensile tests

The monotonic tensile tests are executed on cylindrical specimens designed in accordance with the European standard EN 13674-1 (2011). The specimens are extracted from the rail head, according to the scheme reported in Figure 1. Successively, the specimens are maintained at a temperature of 200 °C for six hours, to relax superficial residual stresses induced by the machining procedure and to improve ductility. A total of four specimens have been tested, two extracted from the right side and two from the left side of the head of the rail. The monotonic tensile tests are executed using an electro-mechanical universal testing machine INSTRON 5985 equipped with a load cell having a nominal capacity of 250 kN. The test is executed by controlling the displacement of the cross-head, translating at a constant speed of 0.75 mm/min which corresponds to $\dot{e_L} = 0.000\ 25\ s^{-1}$. The elongation is measured through the parallel length of the specimen using a contactless extensometer tracking the relative displacement of two marks on the specimen surface, which are initially 50 mm apart. The conditioning and the acquisition of the signals from the load cell, cross-head position, and extensometer are embedded in the controller. A sampling frequency of 10 Hz is used.

2.3. Fatigue crack growth and fracture toughness tests

The tests aiming to quantify the fatigue crack growth rate and plane strain fracture toughness are executed using compact tension C(T) specimens, with dimensions according to the ASTM-E647 ASTM (2008) and ASTM-E399 ASTM (2020), respectively. The specimens are extracted from the center of the rail head with the notch pointing downwards. A total of two and four specimens have been used for each test, respectively. The tests have been executed in a testing frame equipped with a hydraulic actuator and a load cell with a nominal capacity of 125 kN. A closed-loop control system ensures allows the test is controlled using force feedback for both cyclic and monotonic loading. A clip-on displacement transducer - model UB-5A from TML - is mounted directly on the built-in knife edges manufactured at the crack mount with an initial opening of 4.0 mm. The specimen is loaded through clevis and pin, designed according to the aforementioned standards. Moreover, both clevis are connected to the load line using spherical hinges, to ensure that secondary bending moments are minimized. The conditioning and the acquisition of the signals from the loadcell and extensometer are embedded in the controller. The conditioned signals are delivered to a data acquisition system from National Instruments for saving the data. The sampling frequency is set to 300 Hz.

Two tests were conducted to measure the fatigue crack growth rate, using two different load ratios, namely $R = 0.1$ and $R = 0.5$, on C(T) specimens having thickness (B) = 10 mm and width (W) = 40 mm. The cyclic loading for both pre-cracking and fatigue crack growth rate measurement is executed at a constant load range, resulting in an increasing stress intensity factor range. For both specimens, the maximum load was equal to 4.95 kN. However, for the specimen tested at $R = 0.5$ the pre-cracking procedure started by applying $R = 0.1$ up to an initial pre-crack of 1 mm. Successively, the pre-cracking procedure continued with the load ratio $R = 0.5$. During cyclic loading, the crack size measurement is done indirectly using the compliance method and based on the crack mouth opening

displacement measured using the clip-on extensometer, ASTM (2020, 2008). The compliance, u, resulting from crack mount opening displacement, v, is:

$$u = \left[\left(\frac{EvB}{P}\right)^{1/2} + 1\right]^{-1} \tag{1}$$

where E is the Young Modulus and P the applied load. The relative crack depth is calculated as:

$$\frac{a}{W} = 1.0010 - 4.6695u + 18.460u^2 - 236.82u^3 + 1214.9u^4 - 2143.6u^5 \tag{2}$$

with a being the crack depth. To minimize the effect of crack closure on compliance reading, Equation 1 is evaluated when the loading on the descendent branch of the load cycle is at 90% of the amplitude, Fleck (1991). In addition, a crack gauge KYOWA KV-5C with a wire grid pitch of 0.1, and 45 mm gauge, has been used for calibrating the compliance.

Four tests were conducted to measure the linear elastic plane-strain fracture toughness, using C(T) specimens having $B = 20$ mm and $W = 40$ mm. A fatigue pre-crack was induced in the specimens by applying constant amplitude loading characterized by a load ratio $R < 0.1$ and $P_{max} \leq 11$ kN, depending on the specimen. During pre-cracking, the crack size was monitored using compliance measurement based on crack mouth opening displacement, as for the crack growth rate tests, and qualitatively checked during the tests by using a hand-held microscope. The fracture toughness test is executed at room temperature, by increasing the applied load at a constant rate up to fracture, and such that the rate of the increase of the stress intensity factor is limited to 2.5 MPa $\text{mm}^{1/2}$, in accordance with the standard procedure. This was done based on the pre-crack measurement on the surface of the specimen. The load-displacement plot is analyzed following the procedure for determination of the size insensitive fracture toughness, reported in the annex X of the ASTM E399 ASTM (2020). In this procedure, the slope of the secant to the load-displacement curve used to identify the load to be used for fracture toughness determination is dependent on the ligament and not fixed to 95%. This waives the condition for which the maximum load should be not larger than 1.1 P_Q, resulting in a valid test. The secant offset percentage S_Q is a function of the ligament of the crack and for C(T) specimens is:

$$S_Q = 100 - 106/(W - a) \tag{3}$$

and it is related to a constant amount of crack extension, i.e. 0.5 mm, whereas the 95% offset secant is based on a crack extension that is a constant percentage, i.e. 2%, of the final pre-crack size Wells et al. (2018).

2.4. Microscopy analysis

After the tests, the fractured surfaces were cleaned with isopropanol in an ultrasonic bath to remove any dirt and facilitate the observation. The specimens were then first analyzed in low magnification using a Keyence VHX-6000 Light Optical Microscope (LOM). Higher magnification images were obtained using a JEOL IT100 Scanning Electron Microscope (SEM) in secondary electron detection mode at an acceleration voltage of 20 kV, and a working distance of 11 mm. Figure 2 shows the description of the sectioning by wire spark erosion of the tensile specimens after rupture. The first sample (A) was used to analyze the fracture surface as indicated with the white arrow in Figure 2. An additional analysis was made on the tensile sample to investigate the cross-section of the specimen. For that, the specimen was cut in the radial longitudinal section (Figure 2 B). Standard metallographic techniques followed by chemical etching with Nital 2% were performed to reveal the microstructural features.

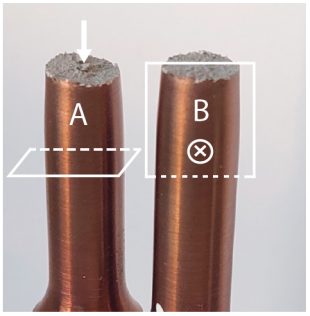

Fig. 2: Sectioning of tensile specimens with a diameter of 10 mm after the rupture in monotonic tensile tests with arrows indicating the observation plane.

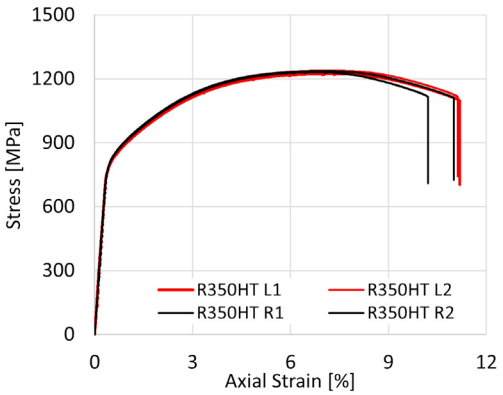

Fig. 3: Uniaxial stress-strain curves obtained from monotonic tensile tests of R350HT specimens.

3. Results

Figure 3 depicts the uniaxial stress-strain curves measured during the monotonic tensile test of four R350HT specimens. It can be observed that up to the ultimate tensile stress the curves are overlapping, denoting a high degree of reproducibility of the tests. The average values of Young's Modulus (E), 0.2% proof stress and Ultimate Tensile Stress (UTS) obtained from the tensile curves are 218.8 (± 6) GPa, 838.5 (± 8) MPa, and 1232 (± 8) MPa, respectively.

The analysis of the fracture surface, presented in Figure 4a, shows that generally a brittle fracture is observed, characterized by typical river patterns highlighted with a white arrow. However, microscopic dimples (black arrow) reveal some ductile areas associated with ductile fracture of pro-eutectoid ferrite present at some grain boundaries.

An examination of the tensile specimens in a radial longitudinal section (Figure 4b) reveals the necking profile and the presence of shear lips in the vicinity of the fracture surface (white arrows). These features are typical of ductile failure and are due to a plane state of stress i.e. shear dominated fracture. Moreover, multiple secondary cracks develop in the bulk of the material, see Figure 4c. These secondary cracks are mainly located in the pro-eutectoid ferrite region, known for being a preferential site for crack nucleation and propagation in railway steels.

The plane strain fracture toughness tests are executed on pre-cracked C(T) specimens, as described in Section 2.3. Table 1 summarizes the results obtained from the fracture toughness tests. An average fracture toughness value of 1100.9 MPa$(mm)^{1/2}$ is obtained from the valid tests. This value is in line with typical fracture toughness values obtained for pearlitic rail steels. Figure 5a shows the interface between the pre-crack zone and the crack propagation zone visible after the monotonic test, which was used to calculate the pre-crack extension from the notch.

In the vicinity of the fatigue pre-crack zone (Figure 5b) it is possible to observe numerous points of initiation of the brittle fracture, which is characterized mostly by a cleavage type of fracture. Furthermore, the presence of ridges in

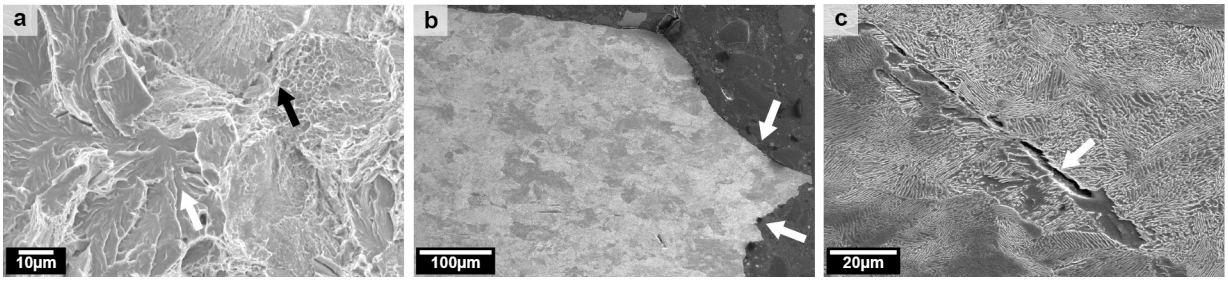

Fig. 4: SEM micrographs of tensile specimens depicting (a) the fracture surface, (b) the radial longitudinal section in the vicinity of the fracture surface, (c) the radial longitudinal section in the bulk.

Table 1: Summary of the test results for the plane strain fracture toughness

Specimen	$P_{max,p}$ [kN]	R_p [-]	a/W [-]	S_Q [%]	P_{Qsi} [kN]	P_{max} [kN]	K_Q [MPa(mm)$^{1/2}$]	K_{Isi} [MPa(mm)$^{1/2}$]
01	11.0	0.10	0.53	94.3	14.4	16.3	1222.3	*
02	9.45	0.10	0.48	94.9	15.1	18.4	1094.1	1094.1
03	11.0	0.05	0.47	94.9	15.5	18.2	1107.4	1107.4
04	10.5	0.05	0.47	95.0	13.4	17.5	956.54	*

(*) invalid test: $P_{max,p}/P_{Qsi} > 0.6$

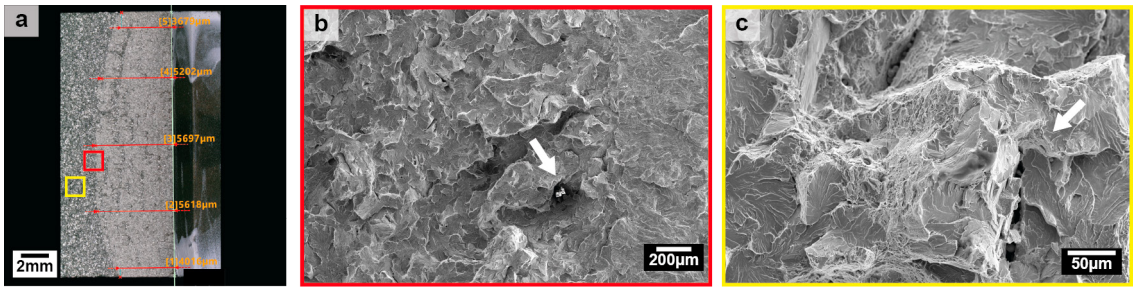

Fig. 5: Microscopy investigation on the C(T) specimen R350HT-20-01. (a) optical micrograph of fracture surface; High magnification SEM micrograph of the fracture surface in (b) the vicinity of the fatigue pre-crack zone (red rectangle) and (c) in the brittle fracture region (yellow rectangle).

the fatigue crack growth region (Figure 5c) denotes brittle crack advancements and intergranular crack growth, which was confirmed by observing longitudinal sections of the C(T) specimen. These regions also account for the presence of ductile regions showing micro-dimples associated with the presence of pro-eutectoid ferrite at the boundaries.

The fatigue crack growth rate curves obtained by testing the specimens R350HT-10-01 and R350HT-10-02 tested under $R = 0.1$ and $R = 0.5$, respectively, are depicted in Figure 6. The curves are plotted together with fatigue crack growth rate curves of two different railway steel grades (900 A and R260) from the literature for comparison. The comparison has been done considering the Paris curve fitted to the results of grade 900A steel, of which the test data have been reported in Christodoulou et al. (2016), for load ratio $R = 0.1$ and $R = 0.5$. It can be deduced that the fatigue crack growth rate for the tested R350HT steel is very similar to the grade 900A rail steel tested by Christodoulou et al. (2016), for both load ratios. In general, a higher fatigue crack growth rate should be expected as compared to R260 rail steel, which confirms the lower damage-tolerant behavior of R350HT rails, despite the fact that R260 and R350HT have very similar chemical compositions.
Figure 7 shows the fracture surface of the fatigue crack growth specimen R350HT-10-01, providing a microscopic image of the fracture surface at relatively low (Figure 7a) and relatively high (Figure 7b) fatigue crack growth rates. The fracture surface shows intergranular fatigue crack growth, confirmed by a microscopy analysis on a longitudinal

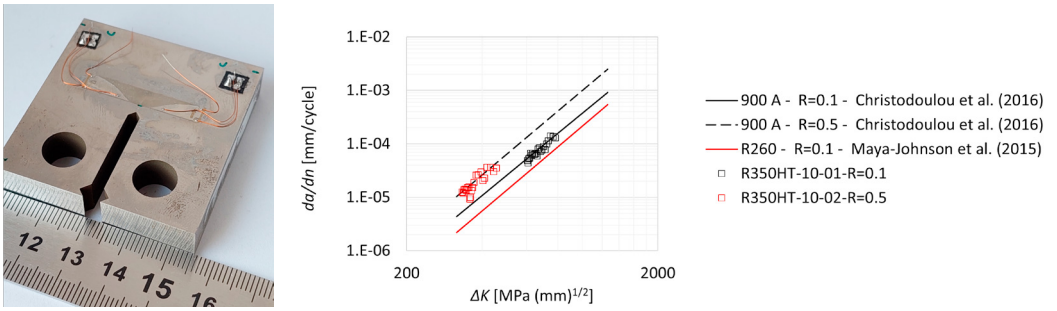

Fig. 6: Fatigue crack growth specimen (left) and fatigue crack growth rates measured in the current study compared with the fatigue crack growth rate curves from Christodoulou et al. (2016) and Maya-Johnson et al. (2015) (right).

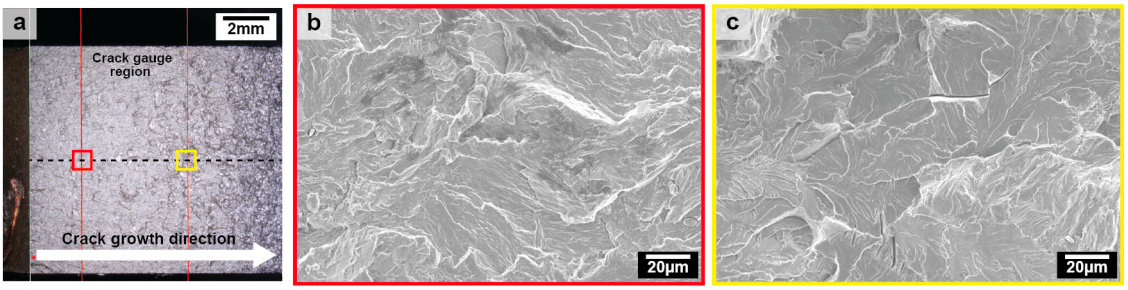

Fig. 7: (a) Optical micrograph of fatigue crack growth surface of specimen R350HT-10-01; Enlarged SEM micrograph of (b) low propagation rate region (red rectangle) and (c) high propagation rate region (yellow rectangle).

section of the specimen. Moreover, through measurement of the distance between focal planes it resulted that at higher fatigue crack growth rates, i.e. at ΔK close to 780 MPa(mm)$^{1/2}$, the fracture surface is more irregular.

4. Conclusions

The paper presents a mechanical characterization of R350HT rail steel, which is a premium-grade steel used in a rail network when higher resistance to wear and yield is required. However, this brings the potential disadvantage of lower damage tolerance, once a crack is nucleated.

Tensile tests and examination of the fracture surface have evidenced the relatively high strength of this steel, which is characterized by a typical brittle fracture behavior at room temperature and under the tested loading rate.

Linear elastic plane strain fracture toughness tests have been conducted on C(T) specimens at room temperature. In particular, the procedure for determining size-insensitive plane strain fracture toughness has been followed, which is based on a fixed crack extension of 0.5 mm. Two valid test results have been reported, with an average value of 1100.9 MPa(mm)$^{1/2}$, in line with typical values of pearlitic rail steels. Fatigue crack growth rate tests have been conducted for two load ratios, namely R = 0.1 and R = 0.5, and a comparison is made with grade 900A and R260 rail steels. It results that the fatigue crack growth rate for R350HT is comparable with that one of grade 900A and higher than R260 rail steel.

Acknowledgements

This research was carried out under project number S16042a and T18014 in the framework of the Partnership Program of the Materials innovation institute M2i (www.m2i.nl) and the Technology Foundation TTW (www.stw.nl), which is part of the Netherlands Organization for Scientific Research (www.nwo.nl). The authors would like to thank Voestalpine Railpro for providing the rail for this research.

References

ASTM, 2008. E647-15 - Standard test method for measurement of fatigue crack growth rates.

ASTM, 2020. E399-20a - Standard Test Method for Linear-Elastic Plane-Strain Fracture Toughness of Metallic Materials.

Bogdanski, S., Olzak, M., Stupnicki, J., 1996. Numerical stress analysis of rail rolling contact fatigue cracks. Wear 191, 14–24.

Bogdański, S., Stupnicki, J., Brown, M.W., Cannon, D.F., 1999. A two dimensional analysis of mixed-mode rolling contact fatigue crack growth in rails, in: European Structural Integrity Society. Elsevier. volume 25, pp. 235–248.

Cannon, D., Pradier, H., 1996. Rail rolling contact fatigue research by the european rail research institute. Wear 191, 1–13.

Christodoulou, P., Kermanidis, A., Haidemenopoulos, G., 2016. Fatigue and fracture behavior of pearlitic grade 900a steel used in railway applications. Theoretical and Applied Fracture Mechanics 83, 51–59.

Christoforou, P., Fletcher, D., Lewis, R., 2019. Benchmarking of premium rail material wear. Wear 436, 202990.

EN 13674-1, 2011. Railway applications. Track. Rail. Vignole railway rails. CEN.

Farjoo, M., Pal, S., Daniel, W., Meehan, P.A., 2012. Stress intensity factors around a 3d squat form crack and prediction of crack growth direction considering water entrapment and elastic foundation. Engineering Fracture Mechanics 94, 37–55.

Fleck, N., 1991. Compliance methods for measurement of crack length. Engineering Materials Advisory Services Ltd., Fatigue Crack Measurement: Techniques and Applications(UK), 1991, , 69–93.

Kapoor, A., 1997. Wear by plastic ratchetting. Wear 212, 119–130.

Leonetti, D., Vantadori, S., 2022a. On the growth of rolling contact fatigue cracks using weight functions. Procedia Structural Integrity 39, 9–19.

Leonetti, D., Vantadori, S., 2022b. Weight functions for stress intensity factor and t-stress derived for an inclined edge crack in a finite width plate. International Journal of Fatigue 165, 107170.

Lichtberger, B., 2011. Track compendium. PMC Media House.

Masoudi Nejad, R., Farhangdoost, K., Shariati, M., 2020. Microstructural analysis and fatigue fracture behavior of rail steel. Mechanics of Advanced Materials and Structures 27, 152–164.

Maya-Johnson, S., Ramirez, A., Toro, A., 2015. Fatigue crack growth rate of two pearlitic rail steels. Engineering fracture mechanics 138, 63–72.

Olzak, M., Stupnicki, J., Wojcik, R., 1991. Investigation of crack propagation during contact by a finite element method. Wear 146, 229–240.

Pucillo, G.P., 2022. The effects of the cold expansion degree on the fatigue crack growth rate in rail steel. International Journal of Fatigue 164, 107130.

Pucillo, G.P., Carrabs, A., Cuomo, S., Elliott, A., Meo, M., 2021. Cold expansion of rail-end-bolt holes: Finite element predictions and experimental validation by dic and strain gauges. International Journal of Fatigue 149, 106275.

Pucillo, G.P., Esposito, L., Leonetti, D., 2019. On the effects of unilateral boundary conditions on the crack growth rate under cycling bending loads. International Journal of Fatigue 124, 245–252.

Rosenfield, A., Hahn, G., Embury, J., 1972. Fracture of steels containing pearlite. Metallurgical and Materials Transactions B 3, 2797–2804.

Trollé, B., Gravouil, A., Baietto, M.C., Nguyen-Tajan, T., 2012. Optimization of a stabilized x-fem formulation for frictional cracks. Finite elements in analysis and design 59, 18–27.

Wells, D.N., James, M.A., Allen, P.A., Wallin, K.R., 2018. A review of the proposed kisi offset-secant method for size-insensitive linear-elastic fracture toughness evaluation. Materials Performance and Characterization 7.

Zerbst, U., Lundén, R., Edel, K.O., Smith, R.A., 2009. Introduction to the damage tolerance behaviour of railway rails–a review. Engineering fracture mechanics 76, 2563–2601.

Zerbst, U., Mädler, K., Hintze, H., 2005. Fracture mechanics in railway applications—-an overview. Engineering fracture mechanics 72, 163–194.